Conductive and Capacitive Properties of the Bipolar Membrane Junction Studied by AC Impedance Spectroscopy†

Antonio Alcaraz

Departament de Ciències Experimentals, Universitat Jaume I, E-12080 Castelló, Spain

Patricio Ramírez

Departament de Física Aplicada. Universitat Politècnica de València, Camino de Vera s/n, E-46022 València, Spain

José A. Manzanares and Salvador Mafé*

Departament de Termodinàmica, Facultat de Física, Universitat de València, E-46100 Burjassot, Spain

Received: April 26, 2001; In Final Form: August 3, 2001

The complete ac impedance spectrum of four bipolar membranes is analyzed both theoretically and experimentally taking into account both ionic transport and water dissociation together with the structural aspects of the bipolar junction. A theoretical model based on the Nernst−Planck and Poisson equations for the conductive and capacitive properties of the junction provides a qualitative description of the bipolar membranes for a broad range of electric currents and temperatures. Special attention is paid to the characteristics of the bipolar junction structure and the contact region between the two ion-exchange layers. It is observed that the effective area of this region increases with the electric current as mobile carriers are extracted from the interface and the layers come in closer contact.

Introduction

Impedance spectroscopy is currently used to characterize a wide variety of electrochemical phenomena concerning solid state, porous materials, synthetic and biological membranes, and liquid electrolytes.[1] Electrical techniques allow for a reproducible "in situ" analysis of the system under operating conditions, in contrast to other techniques that are destructive or need special conditions (X-ray techniques, microscopy, vacuum techniques, electromagnetic waves, etc.).[2] In particular, non-steady techniques such as ac impedance spectroscopy are suitable to investigate complex electrochemical systems. When a small perturbation is applied to the steady state, the electrochemical system follows a relaxation process. As different elementary processes change at different rates, the time response can be analyzed to dissect the overall process.[1−3]

Impedance measurements have been specially useful in the electrochemical characterization of membrane systems. One of the first pieces of evidence for the existence of membranes all around living cells was given by impedance studies.[4] In this paper, the conductive and capacitive properties of polymer ion-exchange bipolar membranes will be analyzed in terms of impedance spectroscopy.

A bipolar membrane (BM) is composed of two ion-exchange layers of opposite fixed charge joined together in series (see Figure 1). This particular arrangement constitutes a model for some biological membranes[1,5] and has also been used as an efficient tool for separation processes (e.g., the production of acids and bases from the corresponding salts by electrodialytic water dissociation.)[6] Theoretical models aimed at describing ion transport in BMs were suggested by Bassignana and Reiss,[7] Coster,[8] Simons,[9] and Zabolotskii,[10] among others.

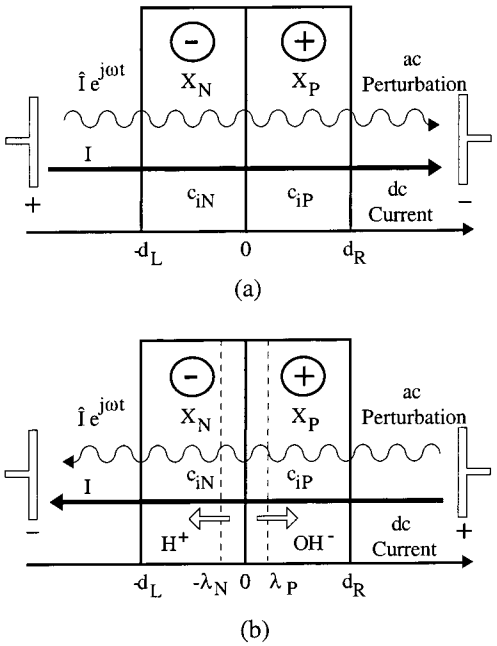

Figure 1. Scheme of the BM under current flow in forward (a) and reverse (b) polarization. The impedance of the BM is obtained by the superimposition of a small ac perturbation of amplitude $\hat{I}$ and angular frequency ω to the dc current I.

The most important BM characteristics in electromembrane processes is the anomalous water dissociation, since the

† Part of the special issue "Howard Reiss Festschrift".

* E-mail: smafe@uv.es.

10.1021/jp011581x CCC: $20.00
Published on Web 09/20/2001

measured fluxes of H^+ and OH^- ions are almost 7 orders of magnitude higher than those that could be expected from ordinary water dissociation.[9] As such large fluxes are not observed in monopolar ion-exchange membranes, it is generally accepted that the high electric field appearing at the bipolar junction (see Figure 1) plays an important role in the water dissociation phenomenon. Previous studies[9,11−12] have shown that this phenomenon takes place when some fixed charge groups (e.g., tertiary amino groups) participating in protonation−deprotonation reactions with the water molecules at the bipolar junction are present in the membrane, although inorganic salts including heavy metals can also show water-splitting properties.[13] Proton transfer in solution is very fast, and the rate-limiting step is the reorganization of water molecules between successive transfers. It has been speculated that the high electric field at the bipolar junction might assist in the transfer of generated protons and hydroxyls.[12,14] The water dissociation in BMs is then considered as an electric field-enhanced (EFE) phenomenon,[7,15] and its magnitude depends critically on the structure and composition of the bipolar junction.[9,14−17] In this context, the studies by Dang and Woermann[15] and Hosono and Tanioka[20] have shown that the efficiency of the generation of protons and hydroxides in BMs changes significantly with increasing the transition region between the two ion-exchange layers.

Previous analysis of the current−voltage ($I-V$) curves under forward and reverse polarization[14] and the membrane potential[18] of BMs have focused on the selectivity and water-splitting capability. Except for the studies of Dang and Woermann[15] and Hosono and Tanioka,[20] these experiments do not provide direct information about the inner structure of the BM junction. In this sense, impedance measurements constitutes a valuable tool for the characterization of the membrane interfacial structure,[21−24] what is crucial to understand the basis of the physical chemistry involved. In the present study, we present a qualitative discussion of the impedance experimental curves, showing that a relative simple model[25] can explain the behavior of several BMs under different conditions of polarization and temperature.

Theory

Transport Equations. The system under study is shown schematically in Figure 1 for the case of the forward ($I > 0$) and reverse polarization ($I < 0$) membrane. The cation-exchange layer contains a fixed negative charge concentration X_N and extends from $x = -d_L$ to 0; the anion-exchange layer has a positive fixed charge concentration X_P and extends between $x = 0$ and d_R. The ion concentrations are denoted by c_{iK}, where $i = 1$ stands for salt cation, $i = 2$ for salt anion, $i = 3$ for the H^+ ion, and $i = 4$ for the OH^- ion. Subscripts L, R, N, and P refer to the ion concentrations in the left and in the right bulk solutions and the cation and anion-exchange layers of the BM, respectively. When a potential drop is established across the membrane under reverse polarization (see Figure 1), the charged species are removed from the interfacial region between the two ion-exchange layers. This region constitutes a space charge zone (depleted electrical double layer) extending from $x = -\lambda_N$ to λ_P. The H^+ and OH^- ions are assumed to be generated in this region via protonation-deprotonation reactions assisted by the high electric field.[7,14]

The system is treated as isothermal and free from convection, and the electrolyte solutions surrounding the BM are assumed to be perfectly stirred (no diffusion boundary layers are taken into account). The ionic transport across the BM is described using the one-dimensional Nernst Planck equations[26]

$$J_{iK} = -D_{iK}\left[\frac{dc_{iK}}{dx} + (-1)^{i+1}c_{iK}\frac{d\Psi}{dx}\right],\ i = 1,..., 4,\ \ K = N, P \tag{1}$$

and the mass conservation is given by continuity equations

$$\frac{\partial J_{iK}}{\partial x} + \frac{\partial c_{iK}}{\partial t} = 0,\ \ i = 1, 2,\ \ K = N, P \tag{2}$$

$$\frac{\partial J_{iK}}{\partial x} + \frac{\partial c_{iK}}{\partial t} = k_d n - k_r c_{3K} c_{4K},\ i = 3, 4,\ K = N, P \tag{3}$$

In eqs 1−3, J_{iK} and D_{iK} denote the flux and the diffusion coefficient of the ith species in the region K (see Figure 1), Ψ is the electrical potential in units (RT/F), where R is the universal gas constant, T is the absolute temperature, and F is the Faraday constant, k_d and k_r are the rate constants of the water dissociation reaction, and n is the concentration of the active groups involved in the process.[14] The boundary conditions necessary to solve these differential equations are provided by the Donnan equilibrium conditions.[7,8]

The EFE water dissociation phenomenon is described in several steps. First, the potential drop across the bipolar junction is estimated by solving the Poisson equation for a totally depleted space charge region[8,14] of typical length of 1−10 nm. Note that under reverse polarization (see Figure 1), the potential drop in the depleted layer of the bipolar junction is much higher than those in the ion-exchange bulk layers and the membrane/solution interfaces. The effect of bipolar junction electric field on the chemical reaction of protonation and deprotonation is taken into account using Timashev's phenomenological approach[16,27]

$$k_d(E) = k_d(0)\exp\left[\frac{\alpha F}{RT}E\right] \tag{4}$$

where k_d (0) refers to the rate constant of water dissociation at the ionizable membrane groups without applied electric field. Equation 4 includes a characteristic length parameter (α is on the order of 10^{-10} m), considered as an effective distance for the dissociation reaction.[16] An interpretation of eq 4 on the basis of simple statistical mechanics has previously been given.[14]

BM Junction Structure. The above description provides a qualitative understanding of $I-V$ curves and membrane potential measurements.[14] When dealing with transport equations, no information about the details of the inner structure of the BM is needed: only the ion-exchange material is relevant and the inert membrane polymer is not considered. Then, the simple picture shown in Figure 1 provides a suitable approximated model. However, modeling of impedance spectra requires considerations about the junction nature.[23] The use of different polymeric matrix, catalysts, and preparation procedures leads to particular interfacial structures.[28,29] Thus, when preformed ion-exchange layers of opposite fixed charge are simply brought together, a relatively smooth interface is formed (see Figure 1). This is the case of bilayer and "sandwich-type" BMs, where the contact area is just the cross-sectional geometric area (A) because the layers do not interpenetrate each other.

However, a corrugated contact region, as shown in Figure 2, is formed when preparation procedures include the use of heterogeneous ion-exchange layers or homogeneous ones with surface heterogeneities.[30] In such cases there is an increase in the contact area between both ion-exchange layers due to surface roughness and the addition of mixed polyelectrolytes or catalysts

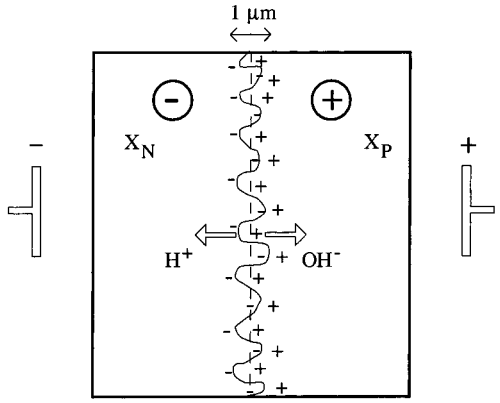

Figure 2. Schematic representation of the contact region in the case of a BM with a corrugated interface. The thickness of this region is on the order of 1 μm. The space charge region extends from both sides of the effective contact plane to some nanometers within the ion-exchange layers.

in the BM junction (compare Figure 2 with Figure 1).[28,29,31] Scanning electron micrographs and X-ray spectrometry show that the typical thickness of the contact region is on the level of micrometers.[20,32] Nevertheless, this distance does not correspond to the space charge layer at the bipolar junction, which is believed to extend from the effective contact zone to some nanometers within the ion-exchange layers.[14] Some indirect evidence can give support to this conclusion. First, it would be impossible to maintain a significant charge separation over a depleted region some micrometers thick (note the enormous electrical resistance that would be associated to this region). Moreover, in a junction of some micrometers (as opposed to nanometers) the typical electric field at the bipolar junction could be reduced by 3 orders of magnitude. Thus, the bipolar junction electric field would be completely irrelevant for the water dissociation reaction in this case, contrary to indirect evidence found in experiments with $I-V$ curves.[9,11,14] The structural modeling of BMs should include information about the contact effective area (A_{ef}). The increase factor $A_{ef}/A > 1$ is not exactly known, but some estimations can be done. An upper limit for A_{ef}/A is given by porous materials, where a value of ca. 10^3 is typical.[33] As ion-exchange membranes are not porous but dense materials, we could anticipate a much lower factor. Another question is the dependence of A_{ef} on the applied voltage. When current increases, more and more mobile carriers are extracted from the bipolar junction (see Figure 1), and both ion-exchange layers come in closer contact, interpenetrating each other. Consequently, A_{ef} is expected to increase with applied current.

Impedance Spectroscopy. The ac impedance characteristics of a BM can be obtained by the superimposition of a perturbation of angular frequency ω on the transport equations. A variable $u(x)$ describing steady-state properties of the system (concentration, flux, electric potential, etc.) becomes now time- and position-dependent, $u(x;t)$. If the amplitude of the perturbation is small enough, the perturbed variable can be written as

$$u(x;t) = u_e(x) + \hat{u}(x)e^{j\omega t} \tag{5}$$

where $\hat{u}(x)$ is the amplitude of the ac response and $j \equiv \sqrt{-1}$. The dc component $u_e(x)$ is assumed to obey steady-state conditions. Due to Donnan exclusion, the concentration of coions (ions with the same sign of charge as the fixed groups) in each ion-exchange layer is low. Therefore, the migration term in the coion Nernst−Planck equations can be neglected. After applying the ac perturbation, we obtain

$$\hat{J}_{iP}(x) \approx -D_{iP}\frac{\partial \hat{c}_{iP}}{\partial x},\ i = 1, 3 \text{ (positive layer)} \tag{6}$$

$$\hat{J}_{iN}(x) \approx -D_{iN}\frac{\partial \hat{c}_{iN}}{\partial x},\ i = 2, 4 \text{ (negative layer)} \tag{7}$$

Under this assumption, the perturbed continuity equations lead to second-order differential equations that can be readily integrated over each ion-exchange layer. The solutions to these equations are connected by the integration of the continuity equations across the bipolar junction. The ac electrical current passing through the system can be evaluated at any point, in particular at the border ($x = \lambda_P$) of the bipolar junction (see Figure 1)

$$\hat{I}(\lambda_P) = F[\hat{J}_{1P}(\lambda_P) - \hat{J}_{2P}(\lambda_P) + \hat{J}_{3P}(\lambda_P) - \hat{J}_{4P}(\lambda_P)] \tag{8}$$

We can obtain now the admittance of the bipolar junction as

$$Y = A\frac{\hat{I}}{\hat{V}} \tag{9}$$

that for a symmetrical BM with $c_{1P}(\lambda_P) = c_{2N}(-\lambda_N)$ and $c_{3P}(\lambda_P) = c_{4N}(-\lambda_N)$ yields

$$Y = \frac{F^2 A c_{2N}(-\lambda_N)}{RT}(1+j)\sqrt{2\omega D_s} + j\omega\frac{\epsilon_r\epsilon_0 A_{ef}}{\lambda} + \frac{F^2 A c_{4N}(-\lambda_N)}{RT}\sqrt{D_w\chi}[\sqrt{a+1} + j\sqrt{a-1}] + \frac{\alpha F A I_d}{RT\lambda} \tag{10}$$

where

$$a \equiv \sqrt{1 + \left(\frac{\omega}{\chi}\right)^2} \tag{11}$$

$$\chi \equiv k_r^0 c_{3N}(-d_L) \tag{12}$$

and I_d corresponds to the current density due to water dissociation.[14] In eqs 10−12, k_r^0 is the rate constant of the recombination of water ions under zero applied voltage and D_s and D_w are the diffusion coefficients for salt and water ions, respectively. Finally, ϵ_r and ϵ_0 are the dielectric constant and the vacuum permittivity, respectively. The full treatment is described in detail elsewhere,[25] and the boundary conditions employed are discussed previously.[22] The complex admittance of eq 10 has four contributions. The first term accounts for the diffusion of salt ions in the membrane layers (the Warburg admittance). The second term reflects the BM junction capacitance due to the charge separation. The third term is the well-known Gerischer admittance describing the simultaneous reaction and diffusion of water ions out of the junction.[10] Finally, the last term is a pure conductance given by the migration of protons and hydroxides produced in the bipolar junction.

Note that the effective contact area A_{ef} only appears in the pure capacitive contribution, since this term reflects the actual structure of the bipolar junction, including membrane supporting inert material. On the contrary, the geometrical area A appears in the other three diffusional and migrational contributions that come from transport equations. In these terms, only the direction of the net current flow is relevant.

3. Experimental Section

Four different BMs were used, one from WSI Technologies Inc. (St. Louis, Missouri) denoted as WSI, one BM from Kuban

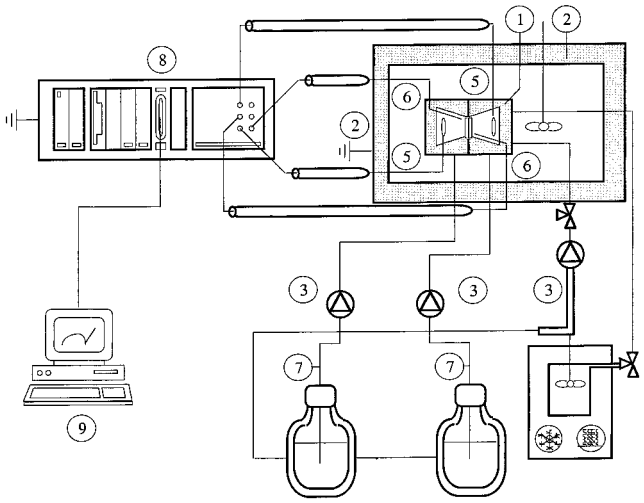

Figure 3. Experimental setup for determination of ac impedance spectra: Measuring cell (1), thermostatic bath (2), pumps (3), thermostat (4), current carrying electrodes (5), reference electrodes (6), salt solutions (7), potentiostat and impedance analyzer (8), and PC data logger (9).

State University (Russia) denoted as MB1[34,35] and two from FuMA-Tech GmbH (St. Ingbert, Germany) denoted as FTBM1 and FTBM2.

The WSI membrane is a bilayer BM composed of separated commercial ion-exchange layers. The anion-exchange layer is a Pall/Raipore R1030 film with strongly basic quaternary ammonium groups, and the cation-exchange layer is a Pall/Raipore R1010 film with sulfonic acid groups. Both films are homogeneous, non-reinforced perfluorinated membranes that show relatively smooth surfaces. The layers were treated previously with solutions containing chromium (III) immobilized as hydroxide.[36,37] The thickness of the anion-exchange layer is ca. 40 μm, and the thickness of the cation-exchange layer is ca. 70 μm.

The MB1 membrane is a sandwich-type BM. The anion-exchange layer is composed of secondary, tertiary, and quaternary amines, and the cation permeable layer contains sulfonic acid groups in polyethylene binder.[38] The structure of the interface is not reported in the literature, although it is known that the BM is formed from preexisting separated ion-exchange layers.[28] The distinctive features of this membrane are the heterogeneous distribution of ionizable groups through the film, and the membrane thickness (ca. 1 mm), approximately 10 times higher than the rest of BMs in this study.

The FTBM-1 membrane has a multilayered structure formed sequentially by casting.[29] An inert screen covers the BM as a reinforcement. The anion-exchange layer contains polysulfone with bicyclic amines, and the cation-exchange layer is made of sulfonated, cross-linked polyether ether ketone.[39] A very thin extra layer (about 10 nm thick) is placed at the intermediate position. It consists of an insoluble polyelectrolyte complex containing tertiary ammonium groups, forming a heterogeneous interface.[29,39] The thicknesses of the layers are approximately 40 (cation-exchange layer) and 20 μm (anion-exchange layer). The FTBM-2 membrane is prepared exactly in the same way as FTBM1, except for the fact that it is non-reinforced.

A scheme of the experimental setup is given in Figure 3. The ac impedance spectra curves were obtained in a four-electrode cell composed of two equal compartments. Two Ag/AgCl plates were used as current electrodes, and the potential drop across the BM was measured using Haber−Luggin capillaries connected to reference electrodes. Multichamber arrangements permit the use of other kind of electrodes nonreversible to the ions in solution that are more stable at low current, but then the previous characterization of the empty cell is much more difficult. The BM was equilibrated for several hours with the solution used in the experiment (0.5 M KCl) before each set of measurements.

The measuring technique is based on the well-known Kelvin four-point method in order to avoid an overlapping of impedance contributions of the current carrying electrodes and the membrane impedance. The experiments were made in a cell specially designed for this purpose composed of two equally sized compartments (see Figure 3).[23] The special geometry of the cell (conical shape) is intended to make the current through the membrane approximately homogeneous, minimizing border effects. The membrane was placed separating the two halves of the cell and equilibrated for several hours with the solution used in the experiment before each set of measurements. A thin rubber ring was arranged together with the membrane, preventing the BM from moving during measurements. The ac impedance spectra curves were obtained using a Zahner IM6 (Zahner Elektrik, Kronach, Germany) impedance analyzer in galvanostatic mode. Each experimental point is taken as the average of 10 acquired points to minimize noise effects. The potentiostat was controlled by a PC computer. To feed the current into the cell under forward and reverse polarization, two Ag/AgCl plates (whose diameters were ca. 3.1 cm) were used, prepared according to a method described in detail elsewhere.[23] The electrodes were renewed every few measurements to keep them in good conditions. The potential was measured using a pair of commercial available Ag/AgCl electrodes (Sensortechnik Meinsberg), each connected to Haber-Luggin capillaries, filled with a 3 mol L^{-1} KCl-saturated solution as salt bridge. The latter were placed in front of each membrane surface (see Figure 3). The distance between the membrane (whose diameter was ca. 10 mm) and the tip of the capillaries was approximately 1.5 mm, and the membrane area was $A = 0.79$ cm^2. The cell was filled with 0.5 mol L^{-1} KCl solutions. The temperature was controlled by the thermostated coiled glass heat exchanger placed between the solution reservoir and the cell. Temperature measurements were made in the solution reservoir and inside the cell, in an effort to avoid thermal gradients. The solution was pumped into each half cell, and the solution stream was directed to the membrane surface so that the necessary stirring was provided to reduce the diffusion boundary layers. After exiting the cell, the solutions were mixed in order to maintain constant their pH values. A first measurement of the cell impedance without membrane was performed to obtain the bulk resistance of the cell, which was calibrated before measurements were made. This previous characterization of the empty cell provided assured us that the cell did not introduce capacitive or inductive contributions in the measured impedance spectra.[22,23]

Results and Discussion

Impedance Spectra at Low Electric Current. In the underlimiting current region, before the water-splitting onset, the concentration of water ions is negligible when compared to salt ions, and only the electrolyte must be taken into account. The bipolar junction still contains a significant amount of mobile carriers, so that no pure capacitive contributions to the admittance are expected because of the screening of the membrane fixed charges by the salt ions. Thus, the impedance spectra corresponds to a linear diffusion phenomenon (the so-called Warburg impedance) produced by salt ions, and the admittance

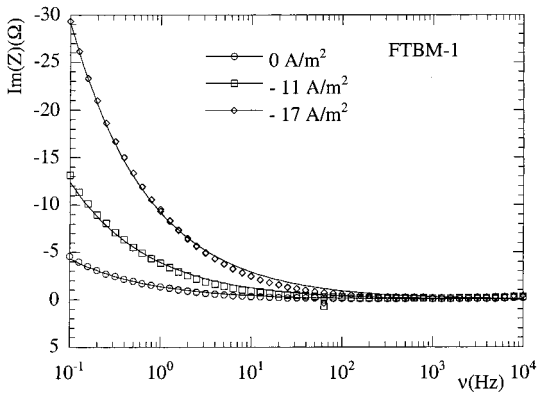

Figure 4. Logarithmic plots of Im(Z) vs ν for FTBM-1 membrane at 298 K for currents under the limiting current. The symbols denote the experimental data under reverse polarization. The solid lines represent the theoretical predictions.

TABLE 1: Values of the Salt Coion Concentration at the Border of the Bipolar Junction, $c_{2N}(-\lambda_N)$, Used To Fit the Experimental Impedance Spectra of FTBM1 Membrane in Figure 4

I (A/m^2)	$c_{2N}(-\lambda_N)$ (mol/m^3)
0	138
−11	48
−17	20

of the system can be described only with the first term of eq 10:

$$Y \equiv F^2 A D_s c_{2N}(-\lambda_N)(1+j)\sqrt{2\omega D_s} \qquad (13)$$

Figure 4 shows the impedance curves for FTBM-1 membrane before the onset of the EFE water dissociation phenomenon. In this case, the resistance rises with increasing current as the bipolar junction becomes a fixed charge region depleted of mobile carriers. Solid lines represent the theoretical predictions of eq 13, with the concentration of salt coion as the only unknown (the diffusion coefficient is taken as $D_s \approx 5 \times 10^{-11}$ m^2/s according to previous studies[14]). The values of $c_{2N}(-\lambda_N)$ used to fit the experimental curves of Figure 4 to eq 13 are shown in Table 1. As could be expected, this concentration decreases with increasing the absolute value of current, showing a reasonable agreement between theory and experiment. Note that under zero current, the concentration in the external border of the bipolar junction can be estimated from Donnan equilibrium, what for this FTBM-1 membrane having $X \approx 1.5$ M,[39] $c_{2N}(-d_L) = c_{2N}(-\lambda_N) = 0.15$ M; which is close to the value obtained for zero current in Table 1.

The impedance spectra of FTBM-2 membrane under forward ($I > 0$) and reverse ($I < 0$) polarization are presented in Figure 5. Forward polarization curves show the same general shape as the reverse polarization ones, except for the fact that the impedance decreases with increasing current because of the accumulation of salt ions at the bipolar junction. These trends are also observed in the values of salt coion concentration used to fit the experimental curves to the theory (see Table 2). Plots of the curves of Figures 4 and 5 in the complex plane (Im(Z) versus Re(Z) curves) show the straight line with 45° slope characteristic of Warburg linear diffusion. Tables 1 and 2 indicate that salt concentration inside the FTBM-2 membrane is similar to that of the FTBM-1.

Although salt diffusion is observed in all studied membranes in the underlimiting region, this is especially noticeable in the FTBM-1 and FTBM-2 membranes, which agrees with the high

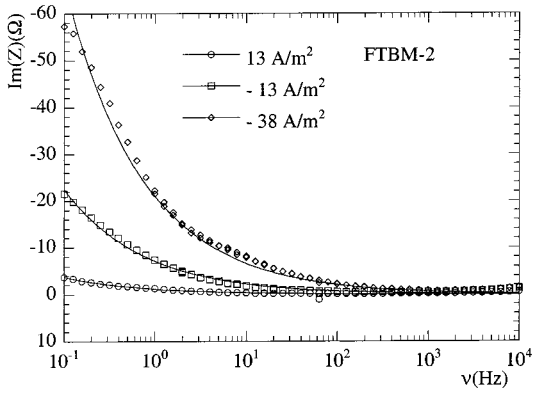

Figure 5. Logarithmic plots of Im(Z) vs ν for FTBM-2 membrane at 298 K for currents under the limiting current. The symbols denote the experimental data under forward and reverse polarization. The solid lines represent the theoretical predictions.

TABLE 2: Values of the Salt Coion Concentration at the Border of the Bipolar Junction, $c_{2N}(-\lambda_N)$, Used To Fit the Experimental Impedance Spectra of FTBM2 Membrane in Figure 5

I (A/m^2)	$c_{2N}(-\lambda_N)$ (mol/m^3)
13	123
−13	26
−38	20

limiting currents observed in the $I-V$ curves of these membranes.[14,40] For the other membranes, the salt diffusion effect is not so apparent, since they have very low limiting currents and salt diffusion is masked by the EFE water dissociation even for low currents (note again that the admittances are connected in series, and thus the major admittance dictates the membrane behavior).[14, 23]

Impedance Spectra at High Electric Current. As the applied voltage increases, the bipolar junction becomes almost depleted of mobile ions, and a limiting current is reached.[7] The space charge region appearing in the junction (see Figure 1) gives rise to the high electric field responsible for the EFE water dissociation. Under these conditions, the admittance of the system is described by the full eq 10, and the four terms in this equation must be considered.

Note also that for high enough electric currents, the effects associated to the water flow to the bipolar junction (in particular the finite value of the membrane mechanical permeability) could not be ignored.[19,41,42] However, we believe that this flow will not change significantly the ac impedance spectra because our experiments are carried out for electric currents below those causing desiccation of the bipolar junction [1,2]. (We know that we are working in this regime because there is no saturation in the current−voltage curves under reverse polarization.[19,41,42] When this saturation is observed, the water flow is not high enough to compensate for the water dissociation at the bipolar junction and irreversible damage of the membrane may result. This is not the case of the experiments reported here whose reproducibility was carefully checked.)

The salt diffusion results are important to estimate the order of magnitude of salt coion concentration. In previous studies of BMs under reverse polarization the contribution of salt coion was neglected against that of the water coions when the current is high enough.[10] However, Tables 1 and 2 show that the concentration of salt coion is always higher than the water coion concentration ($<10^{-7}$ M). Note that the Warburg term depends on the salt coion concentration, whereas the Gerischer term depends on the water coion concentration. Diffusive-type

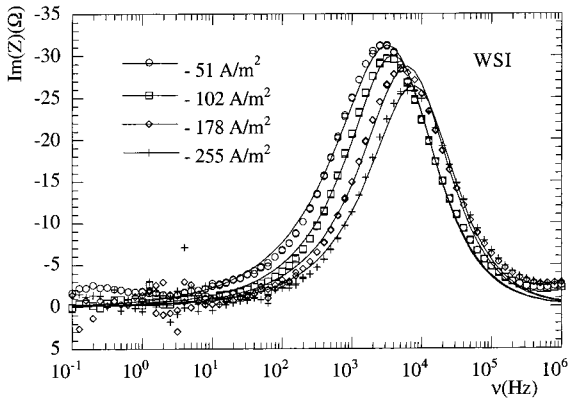

Figure 6. Logarithmic plots of Im(Z) vs ν for WSI membrane at 298 K. The symbols denote the experimental data under reverse polarization. The solid lines represent the theoretical results.

TABLE 3: Values of the Parameters $c_{2N}(-\lambda_N)$, A_{ef}/λ, and α/λ Used To Fit the Experimental Impedance Spectra of WSI Membrane in Figure 6

I (A/m^2)	$c_{2N}(-\lambda_N)$ (mol/m^3)	λ (m) (from A_{ef}/λ)	λ (m) (from α/λ)
−51	8×10^{-3}	4×10^{-8}	1×10^{-9}
−102	6×10^{-3}	4×10^{-8}	4×10^{-9}
−178	4×10^{-3}	5×10^{-8}	9×10^{-9}
−255	4×10^{-3}	5×10^{-8}	1.4×10^{-8}

contributions must come always from coions, since counterion transport is dictated mainly by migration. Water dissociation increases the local concentration of water counterion decreasing then the concentration of coion according to the dissociation equilibrium

$$c_{3N}(-\lambda_N)c_{4N}(-\lambda_N) = k_w \tag{14a}$$

$$c_{3P}(\lambda_P)c_{4P}(\lambda_P) = k_w \tag{14b}$$

where k_w is the equilibrium constant for normal water dissociation. The comparison between the Warburg and the Gerischer terms indicates that the latter is negligible against the first one, and the admittance of the system can be represented by just three terms:

$$Y \equiv \frac{F^2 A c_{2N}(-\lambda_N)}{RT}(1+j)\sqrt{2\omega D_s} + j\omega\frac{\epsilon_r\epsilon_0 A_{ef}}{\lambda} + \frac{\alpha F A I_d}{RT\lambda} \tag{15}$$

Figure 6 shows a logarithmic plot of Im(Z) versus $\nu = \omega/2\pi$ for the WSI membrane in the high current region. The curves (parametric in the electric current and recorded at 298 K) present a maximum at $\nu = \nu_{max}$ that decreases with the absolute value of electric current in reverse polarization. In the limiting current region, there is a transition from the typical linear diffusion behavior of Figures 4 and 5 to the bell-shaped curves of Figure 6.[23] Solid lines in Figure 6 represent the theoretical predictions of eq 15. Taking $A = 7.85 \times 10^{-5}$ m^2, $\epsilon_r = 20$, and $\alpha = 3 \times 10^{-10}$ m,[14] the fitting parameters are the concentration of salt coion in the external border of the junction $c_{2N}(-\lambda_N)$, and the ratios A_{ef}/λ and α/λ. The values used in Figure 6 for these parameters are presented in Table 3. The WSI is a bilayer BM: both ion-exchange layers are joined manually and a thin water layer could be expected to remain at the junction. As each layer presents well-defined smooth surfaces, the effective contact area A_{ef} should be similar to the geometrical area A. However, the lengths of the junction λ appearing in the second and third terms of eq 15 can be different, since the capacitive term reflects the

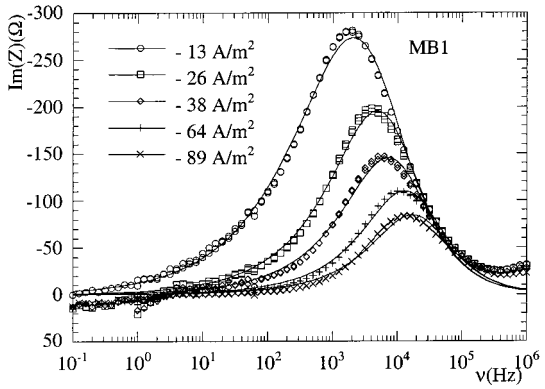

Figure 7. Logarithmic plots of Im(Z) vs ν for MB1 membrane at 298 K. The symbols denote the experimental data under reverse polarization. The solid lines represent the theoretical results.

TABLE 4: Values of the Parameters $c_{2N}(-\lambda_N)$, A_{ef}/λ and α/λ Used To Fit the Experimental Impedance Spectra of MB1 Membrane in Figure 7

I (A/m^2)	$c_{2N}(-\lambda_N)$ (mol/m^3)	λ (m) (from A_{ef}/λ)	λ (m) (from α/λ)
−13	1.3×10^{-3}	3×10^{-7}	4×10^{-9}
−26	1.1×10^{-3}	3×10^{-7}	1.0×10^{-8}
−38	1.0×10^{-3}	3×10^{-7}	1.3×10^{-8}
−64	9×10^{-4}	4×10^{-7}	1.6×10^{-8}
−89	9×10^{-4}	4×10^{-7}	1.7×10^{-8}

actual thickness of the junction (including the neutral water layer and inert supporting material) while the conductive term considers only the ion-exchange material.

The values in Table 3 show the expected decrease of concentration with increasing current, although they must be considered only as crude estimations. Moreover, the junction thicknesses from A_{ef}/λ are significantly larger than those obtained from α/λ. The difference between the values of λ resulting from the second and third terms in the admittance can be explained by the presence of a thin water layer of about 50 nm in the region between both ion-exchange layers.

A similar behavior is expected from MB1 bilayer membrane, formed from separated ion-exchange layers. The comparison between experimental spectra and theoretical predictions from eq 15 is given in Figure 7. The values of the impedance are considerably higher here than in the rest of BMs due to the high membrane thickness (around 1 mm). As both layers are well-defined, we made the same considerations about the fitting parameters as in the case of the WSI membrane ($A_{ef} \equiv A$ and a thin water layer could exist between the ion-exchange layers). The values of the parameters used to fit the experimental curves of the MB1 membrane are shown in Table 4. The concentration of salt coion in the external border of the junction decreases with increasing current, attaining values similar to those in the WSI membrane. The comparison between the capacitive (A_{ef}/λ) and conductive (α/λ) terms indicates that the space charge layer is about 10 nm thick, and that there could be a neutral water layer about 300 nm thick in the intermediate region.

The impedance spectra of the FTBM-1 membrane are shown in Figure 8. The solid lines represent the values given by eq 15 taking into account the fitting parameters of Table 5. As FTBM-1 is a monolayer membrane with a heterogeneous interface, the contact effective area A_{ef} is unknown. Nevertheless, the length of the space charge junction coincides approximately with the actual length of the junction (a few nanometers), since no neutral water layer can appear in this monolayer structure. Thus, we can calculate λ from the fitting parameter α/λ and then estimate A_{ef} from the ratio A_{ef}/λ. The coion concentration

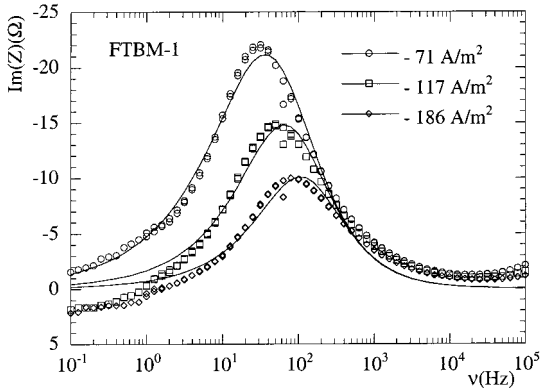

Figure 8. Logarithmic plots of Im(Z) vs ν for FTBM-1 membrane at 298 K. The symbols denote the experimental data under reverse polarization. The solid lines represent the theoretical results.

TABLE 5: Values of the Parameters $c_{2N}(-\lambda_N)$, A_{ef}/λ, and α/λ Used To Fit the Experimental Impedance Spectra of FTBM-1 Membrane in Figure 8

I (A/m^2)	$c_{2N}(-\lambda_N)$ (mol/m^3)	λ (m) (from α/λ)	A_{ef}/A (from A_{ef}/λ)
−71	1.1×10^{-1}	2×10^{-9}	7.4
−117	9×10^{-2}	3×10^{-9}	11.2
−186	8×10^{-2}	4×10^{-9}	12.8

TABLE 6: Values of the Parameters $c_{2N}(-\lambda_N)$, A_{ef}/λ, and α/λ Used To Fit the Experimental Impedance Spectra of FTBM-2 Membrane in Figure 9

I (A/m^2)	$c_{2N}(-\lambda_N)$ (mol/m^3)	λ (m) (from α/λ)	A_{ef}/A (from A_{ef}/λ)
127	1.3×10^{-1}	2.0×10^{-9}	45.8
191	7×10^{-2}	2.5×10^{-9}	52.8
255	6×10^{-2}	2.9×10^{-9}	53.4

values obtained in Table 5 decrease with increasing current and are higher than those obtained in the WSI and MB1 membranes, as could be expected from a less selective membrane with a higher limiting current.[40]

Table 5 shows also the ratio between the effective contact area A_{ef} and the geometrical area A, showing that the heterogeneous interface leads to an increase in the area by a factor of 10. This effective area could increase with current, since both layers can interpenetrate each other more easily as mobile ions are extracted from the junction (without the electrostatic screening effect of these mobile carriers, the fixed charged groups interact more strongly).

The FTBM-2 membrane presents a similar behavior, as is shown in Figure 8 where a considerable scatter in the experimental points appears. These instabilities might be an indication of a decrease in the selectivity of the membrane. As solvated ions permeate into the membrane, polymeric chains become expanded, the water content increases, and the membrane swells. The maxima of the curves of the FTBM-2 membrane are located in the region between 10 and 100 Hz (as occurs also in the FTBM-1 membrane). On the contrary, those of the WSI and MB1 bilayer membranes are in the range 1−10 kHz. This indicates a correlation between the structure of the BM junction and the position of the maxima. Table 6 shows the fitting parameters used to compare theory and experiment. Note that the values of the space charge layer thickness λ, as well as their dependence on the applied current, are almost identical to those obtained for FTBM-1. This fact is not surprising, since the ion-exchange material is the same in both BMs. However, there is a noticeable difference in the capacitive term that leads to higher values of A_{ef} in the FTBM-2 membrane compared to those of the FTBM-1 membrane (A_{ef}/A is now about 50 and increases

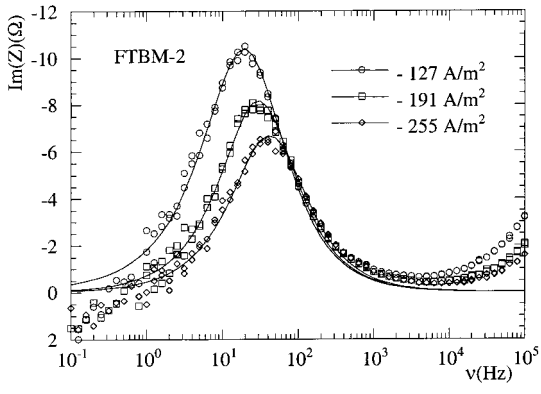

Figure 9. Logarithmic plots of Im(Z) vs ν for FTBM-2 membrane at 298 K. The symbols denote the experimental data under reverse polarization. The solid lines represent the theoretical results.

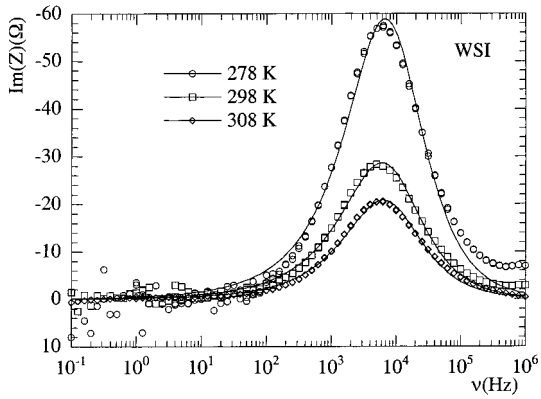

Figure 10. Logarithmic plots of Im(Z) vs ν for WSI membrane under reverse polarization and $I = -178$ A/m^2. The symbols denote the experimental data for three temperatures. The solid lines represent the theoretical results.

with current). The difference between the values of A_{ef}/A for the FTBM-1 and FTBM-2 membranes could be related to the lack of reinforcement of the FTBM-2 and the concomitant membrane swelling. When current increases and the contact region becomes depleted of mobile ions, the screening effects due to these carriers are not present and polymeric chains containing fixed charges of opposite sign interact more strongly. The deformation of polymeric chains should be less inhibited in the FTBM-2 membrane than in the FTBM-1 membrane.

Note finally that it is not in general possible to find an analytical expression giving the position and the height of the maxima in the logarithmic plots of the impedance curves in terms of the model parameters. (Analytical expressions are only possible under simplifying asumptions.[1,10,24,25]) Roughly speaking, the fitting of experimental data to theory appears to indicate that the position of the maxima is dictated essentially by the bipolar junction capacitance, the height of the maximum is given by the water-splitting efficiency (the term containing constant α), and the peak width is determined by the salt contribution term.

Impedance Spectra at Different Temperatures. The effect of temperature on the operation of BMs has been studied in previous approaches using $I-V$ curves.[14] It was shown that increasing the temperature enhances the transport of salt ions across the BM, as well as promotes the water dissociation. The impedance spectra recorded for WSI membrane at different temperatures are shown in Figure 10 where all curves correspond to the same current: $I = -178$ A/m^2. The position of the maxima seems to be almost independent of the temperature,

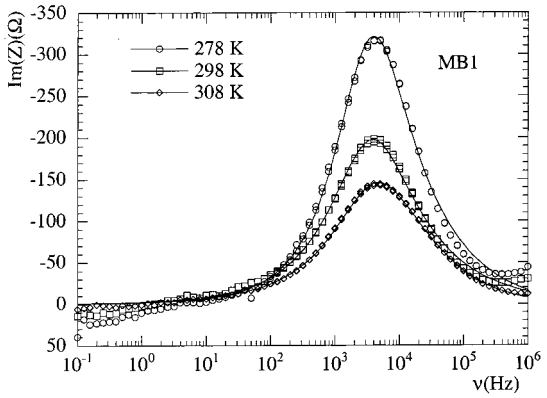

Figure 11. Logarithmic plots of Im(Z) vs ν for MB1 membrane under reverse polarization and $I = -26$ A/m^2. The symbols denote the experimental data for three temperatures. The solid lines represent the theoretical results.

TABLE 7: Values of the Parameters $c_{2N}(-\lambda_N)$, A_{ef}/λ, and α/λ Used To Fit the Experimental Impedance Spectra of WSI Membrane in Figure 10

T (K)	$c_{2N}(\times 96\lambda_N)$ (mol/m^3)	λ (m) (from A_{ef}/λ)	λ (m) (from α/λ)
278	2×10^{-3}	1×10^{-7}	2×10^{-8}
298	5×10^{-3}	5×10^{-8}	1×10^{-8}
308	6×10^{-3}	3×10^{-8}	7×10^{-9}

TABLE 8: Values of the Parameters $c_{2N}(-\lambda_N)$, A_{ef}/λ, and α/λ Used To Fit the Experimental Impedance Spectra of MBI Membrane in Figure 11

T (K)	$c_{2N}(-\lambda_N)$ (mol/m^3)	λ (m) (from A_{ef}/λ)	λ (m) (from α/λ)
278	4×10^{-4}	4×10^{-7}	2×10^{-8}
298	1.0×10^{-3}	3×10^{-7}	1×10^{-8}
308	1.4×10^{-3}	2×10^{-7}	8×10^{-9}

but Im(Z)$_{max}$ decreases with increasing temperature. The values of the fitting parameters used to compare theory and experiment are shown in Table 7. The concentration of salt coion at the BM junction increases with temperature. This can be explained by taking into account that all curves correspond to the same current density. As temperature decreases, it is necessary to apply higher voltages to achieve this current density, and this results in a major extraction of ions from the bipolar junction. The study of the parameters α/λ and A_{ef}/λ shows that λ decreases with temperature. The length of the space charge region λ has no direct dependence on the temperature,[8] but it depends on the applied voltage via the Poisson equation.[14] Since at low temperatures the applied voltage is higher, λ attains higher values, too. The temperature effects on the impedance spectra of MB1 membrane under the reverse current $I = -26$ A/m^2 are shown in Figure 11. Note that the values of Im(Z)$_{max}$ are considerably higher than those of the WSI membrane due to the large thickness of this membrane. The values of the parameters used to fit the experimental curves (see Table 8) show the same trends as those in the WSI membrane.

Conclusions

The complete ac impedance spectrum of BMs is analyzed both theoretical and experimentally by taking into account the basic physicochemical processes involved (ionic transport and water dissociation) together with the structural properties of the bipolar junction. This problem is of interest to both membrane biophysics and membrane technology. First, we have presented a theoretical model based on the Nernst−Planck and Poisson equations and solved it using Donnan equilibrium and local electroneutrality as boundary conditions. We have also discussed the physical meaning of each term in the admittance of the bipolar junction, as well as their relative contribution to the total admittance. Special attention is paid to a question ignored previously: the particular structure of the BM junction under applied current and its contribution to the conductive and capacitive properties of the BM.

The comparison between the theory and experiment shows that the model can provide a qualitative description of four BMs in a broad range of experimental conditions (low and high currents, different temperatures). New information can be obtained on the inner structure of the junction. For instance, ac impedance spectroscopy shows a clear difference between bilayer and monolayer structures. In the former case, a neutral water layer is likely to exist in the intermediate region between the ion-exchange layers. In the latter case, there is an increase in the contact area at the junction due to the interpenetration of both layers. Furthermore, it is argued that the effective contact area increases with increasing current since the layers should come in closer contact as mobile carriers are extracted from the contact region.

Acknowledgment. Financial support from the DGICYT (Project No. PB98-0419), Fundació UJI-Bancaixa (Project P1B98-12), and European Union (Brite-Euram III, project No. BRRT-CT97-5038) are gratefully acknowledged. A.A. and P.R. thank Dr. Hans Holdik (now at FuMA-Tech GmbH; formerly at the University of the Saarland, Germany) for his help with and advice on the experimental part of this paper, and Dr. Bernd Bauer (FuMA-Tech GmbH, Germany) for providing membrane samples.

References and Notes

(1) Coster, H. G. L.; Chilcott, T. C.; Coster, A. C. F. *Bioelectrochem. Bioenerg.* **1996**, *40*, 79.

(2) Gabrielli, C. *Identification of Electrochemical Processes by Frequency Response Analysis*, Pub. No. 004/83; Schlumberger Solartron Electronic Group Ltd., 1984.

(3) Coster, H. G. L.; Chilcott, T. C. The characterization of membranes and membrane surfaces using impedance spectroscopy. In *Surface Chemistry and Electrochemistry of Membranes*; Sørensen, T. S., Ed.; Marcel Dekker: New York, 1999.

(4) Hober, R. *Arch. Ges. Physiol*. **1910**, *133*, 237.

(5) Chilcott, T. C.; Coster, H. G. L. *Ann. NY. Acad. Sci.* **1999**, *873*, 269.

(6) Pourcelly, G.; Gavach, C. Electrodialysis water splitting: Applications of electrodialysis with bipolar membranes (EDBM). In *Handbook on Bipolar Membrane Technology*; Twente University Press: Enschede, 2000.

(7) Bassignana, I. C.; Reiss, H. *J. Membr. Sci.* **1983**, *15*, 27.

(8) Coster, H. G. L. *Biophys. J.* **1965**, *5*, 669.

(9) Simons, R. *Electrochim. Acta* **1984**, *29*, 151.

(10) Zabolotskii, V. I.; Sheldeshov, N. V.; Gnusin, N. P. *Soviet Electrochem.* **1979**, *15*, 1282.

(11) Simons, R. *Electrochim. Acta* **1985**, *30*, 275.

(12) Simons, R. *Nature* **1979**, *280*, 824.

(13) Orthmann, R.; Woermann, D. *Z. Phys. Chem. N. F.* **1986**, *148*, 231.

(14) Mafé, S.; Ramírez, P.; Alcaraz, A.; Aguilella, V. M. Ion transport and water splitting in bipolar membranes: Theoretical background. In *Handbook on Bipolar Membrane Technology*; Twente University Press: Enschede, 2000.

(15) Dang, T.; Woermann, D. *Ber. Bunsen-Ges. Phys. Chem.* **1993**, *97*, 149.

(16) Timashev, S. F.; Kirganova, E. V. *Soviet Electrochem.* **1982**, *17*, 366.

(17) Shimizu, K.; Tanioka, A. *Polymer* **1996**, *38*, 5441.

(18) Higa, M.; Kira, K. *J. Phys. Chem.* **1995**, *99*, 5089.

(19) Aritomi, T.; van den Boomgaard, Th.; Strathmann, H. *Desalination* **1996**, *104*, 13.

(20) Hosono, T.; Tanioka, A. *Polymer* **1998**, *39*, 4199.

(21) Smith, J. R.; Simons, R.; Wiedenhaun, J. *J. Membrane Sci.* **1998**, *140*, 155.

(22) Holdik, H.; Alcaraz, A.; Ramírez, P.; Mafé, S. *J. Electroanal. Chem.* **1998**, *442*, 13.
(23) Alcaraz, A.; Holdik, H.; Ruffing, T.; Ramírez, P.; Mafé, S. *J. Membr. Sci.* **1998**, *150*, 43.
(24) Hurwitz, H. D.; Dibiani, R. *Description of Bipolar Membrane Properties at Steady and Relaxation State*; Conference Proceedings of Electro-Membrane Processes and Bipolar Membrane Technology: Enschede, The Netherlands, 2000; p 14.
(25) Alcaraz, A.; Ramírez, P.; Mafé, S.; Holdik, H. *J. Phys. Chem.* **1996**, *100*, 15555.
(26) Buck, R. P. *J. Membr. Sci.* **1984**, *17*, 1.
(27) Kirganova, E. V.; Timashev, S. F.; Popkov, Y. M. *Sov. Electrochem.* **1984**, *19*, 876.
(28) Wilhelm, F. G.; van der Vegt, N. F. A.; Wessling, M.; Strathmann, H. Bipolar membrane preparation. In *Handbook on Bipolar Membrane Technology*; Twente University Press: Enschede, 2000.
(29) Wilhelm, F. G. Bipolar Membrane Electrodialysis. Membrane Development and Transport Characteristics. Ph.D. Thesis, Twente University Press: Enschede, 2001.
(30) Mizutani, Y. *J. Membr. Sci.* **1990**, *49*, 121.
(31) Wilhelm, F. G.; Pünt, I.; van der Vegt, N. F. A.; Wessling, M.; Strathmann, H. *J. Membr. Sci.* **2001**, *182*, 13.
(32) Krol, J. J. Monopolar and Bipolar Ion Exchange Membranes. Mass Transport Limitations. Ph.D. Thesis, Twente University Press: Enschede, 1997.
(33) Bisquert, J.; Garcia-Belmonte, G.; Bueno, P.; Longo, E.; Bulhoes, L. O. S. *J. Electroanal. Chem.* **1998**, *452*, 229.
(34) *NIITEKhIM. Ion Exchange Membranes, Granular Materials and Powders. (Catalogue)*; Izd. NIITEKhIM: Moscow, 1977.
(35) Zabolotskii, V. I.; Sheldeshov, N. V.; Gnusin, N. P. *Sov. Electrochem.* **1987**, *22*, 1573.
(36) Simons, R. *Bipolar Membrane and Method for Its Preparation*. Australian Patent PCT/AU90/00241.
(37) Simons, R. *J. Membr. Sci.* **1993**, *78*, 13.
(38) Shel'deshov, N. V.; Gnusin, N. P.; Zabolostkii, V. I.; Pis'menskaya, N. D. *Sov. Electrochem.* **1987**, *22*, 742.
(39) Bauer, B. *Bipolar Multilayer Membranes*; Fraunhofer-Gesellschaft zur Förderung der angewandten Forschung eV (FhG), DE 4026154, 1992.
(40) Alcaraz, A.; Ramírez, P.; Mafé, S.; Holdik, H.; Bauer, B. *Polymer* **2000**, *41*, 6627.
(41) Krol, J. J.; Hansink, M.; Wessling, M.; Strathmann, H. *Sep. Purif. Technol.* **1998**, *14*, 41.
(42) Pivovarov, N. Y.; Greben, V. P. *Sov. Electrochem.* **1991**, *26*, 1002.